Taylor & Francis
Taylor & Francis Group

Combustion Theory and Modelling

ISSN: 1364-7830 (Print) 1741-3559 (Online) Journal homepage: https://www.tandfonline.com/loi/tctm20

State-to-state chemical kinetic mechanism for HF chemical lasers

Hui Li, Tianliang Zhao, Jiaxu Li, Shuqin Jia, Dongzheng Yang, Ying Huai, Zhigang Sun, Daiqian Xie, Liping Duo & Yuqi Jin

To cite this article: Hui Li, Tianliang Zhao, Jiaxu Li, Shuqin Jia, Dongzheng Yang, Ying Huai, Zhigang Sun, Daiqian Xie, Liping Duo & Yuqi Jin (2020) State-to-state chemical kinetic mechanism for HF chemical lasers, Combustion Theory and Modelling, 24:1, 129-141, DOI: 10.1080/13647830.2019.1662490

To link to this article: https://doi.org/10.1080/13647830.2019.1662490

Combustion Theory and Modelling, 2020
Vol. 24, No. 1, 129–141, https://doi.org/10.1080/13647830.2019.1662490

State-to-state chemical kinetic mechanism for HF chemical lasers

Hui Li [a,b], Tianliang Zhao[a], Jiaxu Li[a,b], Shuqin Jia[a], Dongzheng Yang[d], Ying Huai[a]*, Zhigang Sun[c], Daiqian Xie[d], Liping Duo[a] and Yuqi Jin[a]

[a]*Key Laboratory of Chemical Lasers, Dalian Institute of Chemical Physics, Chinese Academy of Sciences, Dalian, People's Republic of China;* [b]*University of Chinese Academy of Sciences, Beijing, People's Republic of China;* [c]*State Key Laboratory of Molecular Reaction Dynamics, Dalian Institute of Chemical Physics, Chinese Academy of Sciences, Dalian, People's Republic of China;* [d]*Institute of Theoretical and Computational Chemistry, School of Chemistry and Chemical Engineering, University of Nanjing, Nanjing, People's Republic of China*

(*Received 14 March 2019; accepted 20 August 2019*)

State-to-state rotational relaxation processes play a critical role in predicting rotational nonequilibrium, which can significantly affect total laser power and spectral distribution. In this paper, the state-to-state rotational relaxation rate coefficients for the pumping reaction of F + H_2, the rotational energy transfer processes of HF(υ, j = 0–10) + HF(υ', j' = 0–10) and HF(υ, j = 0–10) + H_2 are calculated. Subsequently, a detailed state-to-state chemical kinetic mechanism is constructed including 61 species and 124,482 elementary reactions for HF chemical lasers. All of these rotational relaxation rate coefficients have been expressed with Arrhenius-like formulas. A comparison of the Boltzmann distribution model with the detailed state-to-state chemical mechanism has been analysed and discussed. These results show that rotational nonequilibrium processes can significantly affect the distribution of ro-vibrational excited HF molecules. The rotational distributions of HF(υ = 0–2, j) are far from equilibrium distribution. Conversely, the distributions of HF(υ = 3, 4, j) seem to be a Boltzmann distribution. These results indicate that numerical models must include the rotational nonequilibrium processes and numerical models using a Boltzmann distribution for the rotational populations cannot predict performance of real HF chemical lasers.

Keywords: State-to-state model; chemical lasers; rotational nonequilibrium; chemical kinetics

1. Introduction

Combustion driven supersonic continuous-wave hydrogen fluoride (HF) and deuterium fluoride (DF) chemical lasers using the hypersonic low-temperature (HYLTE) nozzle have been extensively studied. The mid-infrared HF chemical lasers operate from the fundamental (2.7 µm) and the overtone (1.3 µm) wavelengths. High-energy HF chemical lasers have always been a hot spot in fundamental laser research [1,2] and large-scale laser technology [3] owing to their advantage of being able to generate extremely high power and highly efficient conversion of chemical energy into laser radiation. However, from the chemical point of view, some significant fundamental issues remain ambiguous, such as

*Corresponding author. Email: huaiying@dicp.ac.cn

the rotational nonequilibrium and the poor chemical kinetic model. The presence of rotational nonequilibrium in HF chemical lasers has confused many researchers. To gain better insight into aforementioned key issues, two important questions should be answered [4]: (1) which chemical processes can produce rotational nonequilibrium, and (2) What are the conditions in which rotational nonequilibrium processes exert significant influences.

In a HF chemical laser system, every exothermic chemical process may lead to rotational nonequilibrium, which was first evidenced in pulsed initiated HF lasers [5] and in continuous-wave HF chemical lasers [6]. In the review paper [4], the presence of rotational nonequilibrium and two possible types of chemical processes that produce the nonequilibrium distribution were discussed. The first type of chemical process is the pumping reaction of $F + H_2$ and $H + F_2$ that determine the nascent rotational population. A series of experimental and numerical results have been published, and these results have demonstrated that the nascent distribution of the product of HF(υ, j) is far from equilibrium Boltzmann distribution [7–10]. The second type of process that also contributes significantly to rotational nonequilibrium is the collisional energy transfer processes involving HF(υ, j). However, these rotational state-to-state rate coefficients have not been obtained because of the complexity and difficulty of direct measurements. Therefore, most of the rotational nonequilibrium models depend on theoretical prediction and some experience assumptions. In recent year, the HF molecule as a key tracer of molecular hydrogen in diffuse interstellar medium attracts more attention [11]. These processes of the rotational energy transfer of HF(υ, j) + M have been calculated through the development of experimental apparatus and the use of molecular reaction dynamics, for: HF(υ, j) + He [12], HF(υ, j) + H [13], and HF(υ, j) + H_2 [14,15]. All the above-mentioned results inspire the search for further understanding of HF chemical laser performance.

State-to-state simulation is a powerful numerical tool used to achieve insight into rotational nonequilibrium by considering each rotational level. Several rotational state-to-state chemical kinetic models have been developed to reproduce multi-line lasing, the major evidence of rotational nonequilibrium. Kerber [5] proposed a chemical kinetic model that replaced rotational equilibrium distribution by a near resonant multi-quantum V-R processes to yield highly excited rotational states to analyze the effect of rotational nonequilibrium on output power in pulse chemical lasers. Sentman [6,16] developed a mechanism to describe the presence of rotational nonequilibrium in continuous-wave (cw) HF/DF chemical lasers. Hall [17] reported the rotational nonequilibrium effects on performance loss and multiline resonator spectra in cw HF chemical lasers with a 'exponential gap' model. Despite some simplification and limitations of these models, all of them are more suitable for predicting HF laser performance than the rotational equilibrium model. These latter mechanisms, which were based on a 1976 package devised by Cohen [18], contain numerous erroneous and out-of-date rate coefficients. To date, Manke and Hager [19] have reviewed and updated another vibrational-resolved mechanism for HF chemical lasers. Obviously, chemical kinetic models including rotational nonequilibrium have an outstanding advantage in analyzing spectral distribution and output power. Unfortunately, there are no strong evidences of the presence of the rotational nonequilibrium in real, as opposed to simulated, HF chemical lasers based on both experimental results and theoretical analysis.

The major objective of this paper is to devise a detailed rotational state-to-state chemical mechanism to identify the chemical processes that can produce rotational nonequilibrium. In this work, the rotational relaxation rate coefficients of the pumping reaction of $F + H_2$, HF(υ, j) + HF(υ', j') and HF(υ, j) + H_2(υ) are presented with molecule reaction

dynamics methods in Section 2. A series of numerical simulations are executed separately with the detailed state-to-state mechanism and the skeletal mechanism with the assumption of equilibrium Boltzmann distribution. Subsequently, these numerical results are obtained and discussed in Section 3. Finally, a summary, conclusions and suggested future directions are given in Section 4.

2. Chemical kinetic model

The detailed rotational state-to-state chemical kinetic mechanism presented here is based on the previous mechanism of HF chemical lasers [19]. The vibrational-resolved mechanism includes 15 species and 130 elementary reactions. A complete rotational state-to-state chemical kinetic mechanism has been constructed with 94 species and 368,425 reactions even if the maximum number of rotational levels reaches up to 10. Obviously, it is almost impossible and not necessary to execute numerical simulations because of the huge computational costs. Therefore, a skeletal mechanism is imperative to identify important reaction steps that can lead to rotational nonequilibrium. And the corresponding numerical simulations have been finished in our previous works [20]. The skeletal mechanism is presented in Table 1 including 11 species and 62 elementary reactions. In the present work, the detailed rotational state-to-state chemical kinetic model includes the dominant processes such as $F + H_2 \rightarrow HF(\upsilon, j) + H$, $HF(\upsilon, j) + HF(\upsilon', j')$ and $HF(\upsilon, j) + H_2(\upsilon)$ to account for the processes of rotational relaxation. The rate coefficients of the rest elementary reactions have been recalculated with the assumption of Boltzmann distribution. Finally, a detailed state-to-state chemical kinetic model was devised consisting of 61 species (H, H_2, F, F_2, $HF(\upsilon = 0\text{–}4, j = 0\text{–}10)$, N_2, DF) and 124,482 reactions. The detailed mechanism, given in an Arrhenius-like format $k(T) = A\ T^{\beta}\ exp(-E_a/k_BT)$ and the thermodynamic data, are detailed in the next subsection.

Table 1. Primitive reactions in HF chemical lasers ($\upsilon = 0\text{–}4, j = 0\text{–}10$).

$F + H_2 \rightarrow HF(1, j) + H$	$H + F_2 \rightarrow HF(0, j) + F$
$F + H_2 \rightarrow HF(2, j) + H$	$H + F_2 \rightarrow HF(1, j) + F$
$F + H_2 \rightarrow HF(3, j) + H$	$H + F_2 \rightarrow HF(2, j) + F$
$H + F_2 \rightarrow HF(3, j) + F$	$H + F_2 \rightarrow HF(4, j) + F$
$H + HF(3, 0) \rightarrow F + H_2$	$HF(4,0) + H \rightarrow H_2 + F$
$HF(\upsilon, j) + H_2 \rightarrow HF(\upsilon - 1, j') + H_2$	$HF(\upsilon, j) + F_2 \rightarrow HF(\upsilon - 1, j') + F_2$
$HF(\upsilon, j) + F \rightarrow HF(\upsilon - 1, j') + F$	$HF(\upsilon, j) + DF \rightarrow HF(\upsilon - 1, j') + DF$
$HF(\upsilon, j) + N_2 \rightarrow HF(\upsilon - 1, j') + N_2$	$HF(\upsilon, j) + H \rightarrow HF(\upsilon - 3, j') + H$
$HF(\upsilon, j) + H \rightarrow HF(\upsilon - 2, j) + H$	$HF(3, j_1) + HF(0, j_2) \rightarrow HF(2, j_1') + HF(0, j_2'')$
$HF(1, j_1) + HF(0, j_2) \rightarrow HF(0, j_1') + HF(0, j_2'')$	$HF(1, j_1) + HF(1, j_2) \rightarrow HF(2, j_1') + HF(0, j_2'')$
$HF(2, j_1) + HF(0, j_2) \rightarrow HF(0, j_1') + HF(0, j_2'')$	$HF(3, j_1) + HF(2, j_2) \rightarrow HF(4, j_1') + HF(1, j_2'')$
$HF(4, j_1) + HF(0, j_2) \rightarrow HF(3, j_1') + HF(0, j_2'')$	$HF(2, j_1) + HF(2, j_2) \rightarrow HF(3, j_1') + HF(0, j_2'')$
$HF(2, j_1) + HF(2, j_2) \rightarrow HF(3, j_1') + HF(1, j_2'')$	$HF(3, j_1) + HF(0, j_2) \rightarrow HF(4, j_1') + HF(0, j_2'')$
$HF(3, j_1) + HF(3, j_2) \rightarrow HF(4, j_1') + HF(2, j_2'')$	$F + F + M \rightarrow F_2 + M$
$H + H + M \rightarrow H2 + M$	$F_2 + M \rightarrow F + F + M$

2.1. *F + H₂*

The pumping reaction F + H_2 is a prototypical system for fundamental molecular reaction dynamics in both theoretical and experimental state-to-state reactive scattering studies. In HF chemical lasers, these pumping processes are straightforward to determine the nascent distribution of the product HF(υ, j). In this study, the differential and integral cross sections for F + H_2(υ, j) → HF(υ', j') + H have been calculated to identify the nascent rotational distribution by Sun's and Zhang's group [21,22] with an *ab initio* full dimensional potential energy surface (PES) [23]. Sun [24] reviewed the development PES and quantum dynamics methods for F + H_2 and F + HD, and these results illustrate the high-resolution experimental measurement data validated by Yang's group [1,25–27] with crossed molecular beam apparatus. The initial rotational resolved reaction rate coefficients have been calculated by thermally averaging the translational energies of the corresponding cross section as:

$$k_{\upsilon 0 j_0}(T) = \left(\frac{8k_BT}{\pi\mu}\right)^{1/2}(k_BT)^{-2}\int_0^\infty Ee^{-E/k_BT}\sigma_{\upsilon 0 j_0}(E)\mathrm{d}E, \tag{1}$$

where k_B is Boltzmann's constant, E the translational energy, μ the reduced mass, and $\sigma_{\upsilon 0 j 0}$ the cross section. Finally, the rotational rate coefficients F + H_2 → HF(υ, j) + H were calculated from the Boltzmann averaging of the initial state specific reaction rate constants by Eq.(2).

$$k(T) = \frac{\sum_{\upsilon 0 j 0}(2j_0+1)k_{\upsilon 0 j 0}(T)e^{-E_{\upsilon 0 j 0}/k_BT}}{\sum_{\upsilon 0 j 0}(2j_0+1)e^{-E_{\upsilon 0 j 0}/k_BT}}, \tag{2}$$

where $E_{\upsilon 0 j 0}$ is the ro-vibrational energy of the diatom molecule, and j the rotational quantum number.

The rotational state-to-state rate constants at temperature of 300 K of υ = 1–3, j = 12 are 2.137×10^{11} cm^3 mol^{-1} s^{-1}, 3.949×10^{11} cm^3 mol^{-1} s^{-1} and 3.810×10^{6} cm^3 mol^{-1} s^{-1}, respectively. The rotational state-to-state rate coefficients at T = 300 K are presented in Figure 1. The nascent product distribution is also analysed in Figure 1, which illustrates that the distribution is a partial deviation from Boltzmann distribution at υ = 1–2. However, the nascent distribution of HF(3, j) agrees with the equilibrium Boltzmann distribution. For the vibrational mechanism, the vibrational-resolved rate coefficients have been calculated by sum of each ro-vibrational levels rate coefficients. The weight of vibrational levels distribution is 0.01:0.12:0.51:0.36 for υ = 0–3, which is consistent with the results in Manke's review [19].

2.2. *HF + HF and HF + H₂*

The main relaxation processes in the HF chemical lasers are HF self-relaxation and the V-V energy transfer processes, which can lead to rotational nonequilibrium. The energy transfer process of V, T-R are the most important and significantly contribute to rotational nonequilibrium [6,19]. To provide more information on rotational relaxation behaviour, a full-dimensional *ab initio* PES for the H_2 _ HF and HF – HF *van der Waals* complex was constructed by employing the coupled-cluster singles and doubles with noniterative inclusion of connected triples with an augmented correlation-consistent polarised valence quadruple-zeta basis set plus bond functions. Thus, the rotational state-to-state scattering dynamics for pure rotational and ro-vibrational energy transfer processes were calculated

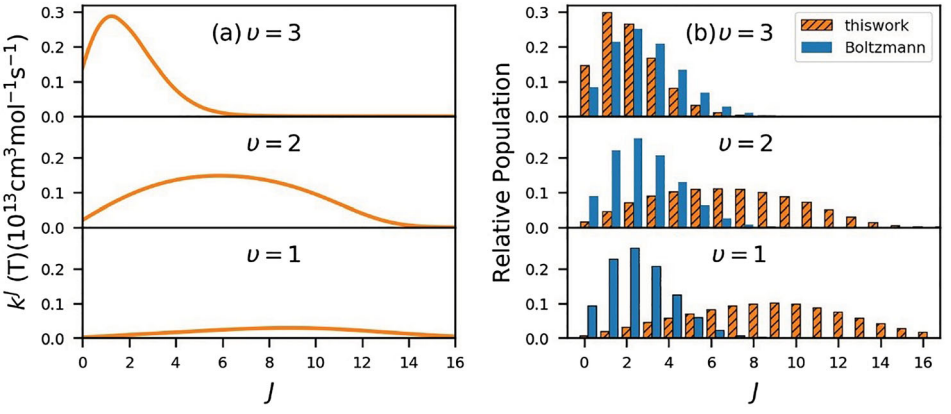

Figure 1. Nascent rotational distribution of F + H_2, where J is the rotational quantum number, (a) Rotational rate constant of HF(υ = 1, 2, 3, j) at T = 300 K. (b) Comparison of nascent distribution and equilibrium Boltzmann distribution. These rate constants have been normalised so that the sum of rotational populations for each vibrational level equals unity.

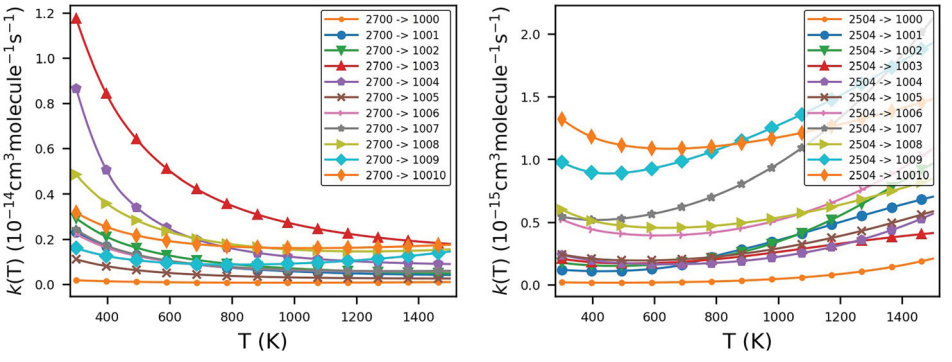

Figure 2. Rotational rate coefficients of HF(υ, j) + HF(υ', j'): (a) rotational deactivation rate coefficients of HF(2, 7) + HF(0, 0) → HF(1, 0) + HF(0, j) as a function of temperature and (b) rotational deactivation rate coefficients of HF(2,5) + HF(0, 4) → HF(1, 0) + HF(0, j).

using the improved coupled-states approximation including the nearest neighbour Coriolis couplings, which are well discussed in [15,28,29].

A new full dimensional *ab initio* intermolecular PES has been developed for HF(υ, j) + HF(υ', j') [30]. In the present case, Figure 2 shows the corresponding rotational rate coefficients as a function of temperature. These rate coefficients for HF(2, 7) + HF(0, 0) decrease monotonously as the temperature increases. Conversely, the rotational rate coefficients for HF(2, 5) + HF(0, 4) increase as the temperature increases. Meanwhile, the vibrational-resolved rate coefficients have been recalculated by Eq.(2), and then by the sum of all of the rotational state-to-state rate constants of products. These corresponding vibrational-resolved rate coefficients are shown in Figure 3. However, there are no sufficient results to validate these types of processes because of their extreme complexity and difficulty. Manke [20] recommended only a measured rate constant $k(300\,\mathrm{K}) \sim 1.87 \times 10^{13}\,\mathrm{cm^3\,mol^{-1}\,s^{-1}}$ and Cohen [18] reviewed $k(300\,\mathrm{K}) = 1.2 \times 10^{13}\,\mathrm{cm^3\,mol^{-1}\,s^{-1}}$ for HF(1) + HF(1) → HF(2) + HF(0),

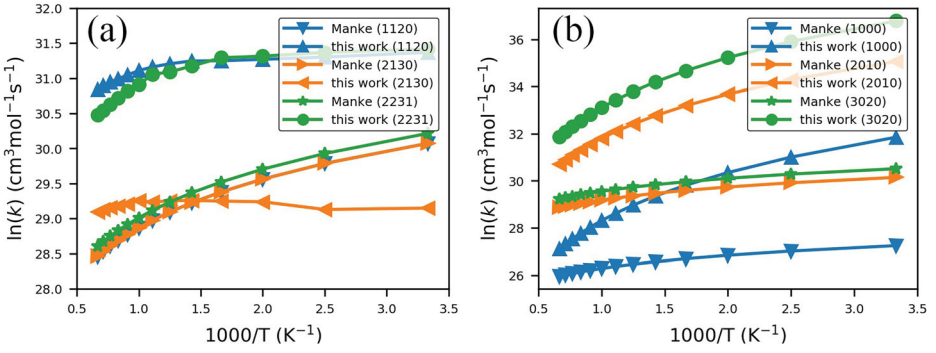

Figure 3. Comparison of results [20] and temperature dependence of rate coefficients. Symbol lines represent the results in this work, and coloured lines represent different types of reaction processes. Vibrational rate coefficients of (a) V-V energy transfer and (b) for HF self-relaxation.

approximately equal to rate constant $k(300\,\mathrm{K}) = 6.689 \times 10^{13}\,\mathrm{cm^3\,mol^{-1}\,s^{-1}}$ that we calculated. The rate coefficients, $6.557 \times 10^{13}\,\mathrm{cm^3\,mol^{-1}\,s^{-1}}$, for HF(2, 2 $\rightarrow$ 3, 2) that we obtained has a good agreement with $4.498 \times 10^{12}\,\mathrm{cm^3\,mol^{-1}\,s^{-1}}$ [18] and $1.69 \times 10^{13}\,\mathrm{cm^3\,mol^{-1}\,s^{-1}}$ [19] at $T = 300\,\mathrm{K}$. However, the self-relaxation processes of HF(υ, j) are greater than one more order of magnitude than those Manke's recommended especially at lower temperature. A well-documented review [4] reported that the rotational rate constants for HF(1, j_1) + HF(1, j_2) $\rightarrow$ HF(1, j_1') + HF(1, j_2'') at a temperature of 300 K is $j_1 = 7$, $j_2 = 15$ approaching $4.6 \times 10^{11}\,\mathrm{cm^3\,mol^{-1}\,s^{-1}}$. All of these V-T, R energy transfer processes need further study to measure these highly uncertain rates.

2.3. *Thermodynamic properties of ro-vibrational excited medium*

The thermodynamic properties of partial HF chemical lasers are summarised in Table 2. Standard enthalpies of formation, entropies and specific heats of the ground state are adopted from the NIST kinetic database [31]. In high power HF chemical lasers, the ro-vibrational excited HF(υ, j) molecules are usually treated as a separated physical species, and the corresponding enthalpies calculated by adding the ro-vibrational energies to the enthalpies of formation of HF(υ, j) molecule. The enthalpy can be defined as

$$\Delta H(\upsilon, j) = \Delta H(0,0) + E(\upsilon, j) - E(0,0), \tag{3}$$

where *ΔH(0, 0), E(0,0)* is the standard enthalpy of formation and ro-vibrational energy of ground state HF molecules. In this study, the first vibrational energy level has been chosen to be the zero of energy to calculate the vibrational partition function of HF(υ, j) [32]. The ro-vibrational energy of the diatom molecule was calculated by Eq.(4):

$$E_{\upsilon,j} = \omega_e\left(\upsilon + \frac{1}{2}\right) - \omega_e x_e\left(\upsilon + \frac{1}{2}\right)^2 + B_\upsilon(j+1) - D_\upsilon j^2(j+1)^2, \tag{4}$$

where $B_\upsilon = 1 - \alpha\ (\upsilon + 1/2)$, and B_υ and D_υ is the rotational constant and the centrifugal distortion constant of HF molecules, respectively [33]. According to the statistical thermodynamic theory of the thermally perfect gas, translation makes a great difference in entropy and the constant volume heat capacity, vibrational motion and rotational motion

Table 2. Standard enthalpy and entropy of HF(υ, j) in chemical lasers.

Species	$\Delta H^{\Theta}{}_{298}$ kJ/mol	$S^{\Theta}{}_{298}$ J K^{-1} mol^{-1}	Species	$\Delta H^{\Theta}{}_{298}$ J K^{-1} mol^{-1}	$S^{\Theta}{}_{298}$ J K^{-1} mol^{-1}
HF(0, 0)	– 273.000	173.78	HF(1, 0)	– 225.944	173.78
HF(0, 1)	– 272.808	173.78	HF(1, 1)	– 225.471	173.78
HF(0, 2)	– 271.823	173.78	HF(1, 2)	– 224.527	173.78
HF(0, 4)	– 268.392	173.78	HF(1, 4)	– 221.226	173.78
HF(0, 6)	– 263.016	173.78	HF(1, 6)	– 216.059	173.78
HF(0, 8)	– 2555.726	173.78	HF(1, 8)	– 209.053	173.78
HF(0,10)	– 246.556	173.78	HF(1, 10)	– 200.245	173.78
HF(2, 0)	– 180.740	173.78	HF(3, 0)	– 137.255	173.78
HF(2, 2)	– 179.380	173.78	HF(3, 2)	– 136.386	173.78
HF(2, 4)	– 176.212	173.78	HF(3, 4)	– 133.351	173.78
HF(2, 6)	– 171.255	173.78	HF(3, 6)	– 128.592	173.78
HF(2, 8)	– 164.533	173.78	HF(3, 8)	– 122.165	173.78

have almost no effect. All of these thermochemical data are fitted with the FITDAT utility [34].

3. Results and discussion

The above described detailed state-to-state chemical mechanism including 61 species and 124,482 reactions was devised along with a skeletal mechanism, consisting of 11 species and 62 reactions, to compare with the assumption of Boltzmann distribution for rotational population in HF chemical lasers [20]. The CHEMKIN-PRO software package [34] was used to gain insight into the processes of the state-to-state chemical mechanism. Comparisons of these two mechanisms are presented and discussed in the following subsection.

3.1. *Major difference of state-to-state model*

Numerical simulations were performed using a closed homogeneous reactor model involving a constant volume with the detailed state-to-state chemical mechanism and the skeletal chemical mechanism. In addition, the initial pressure ranged from 650 to 3,900 Pa, and the initial temperatures were 300 and 500 K. The evolution of the detailed rotational model and the previous numerical models with Boltzmann distribution [19] were carried out.

In Figure 4a, the slope of the temperature is slightly greater than that of the detailed model. The difference value of the maximum temperature value is less than 100 K. However, the evolution of H, H_2, F is in better agreement with these two models. For $F + H_2 \rightarrow HF(\upsilon, j) + H$ and $H + F_2 \rightarrow HF + F$, it is clear to know that the variation of temperature results from rotational level relaxation processes of HF(υ, j). Actually, rotational distribution depends on each vibrational level, and a common way to present the effect on vibrational level is summing the mole fraction of each rotational level. As seen in Figure 4b, the total mole fraction of HF remains almost unchanged. However, values for vibrational excited HF(1) and HF(2) are both lower than the results of Boltzmann's model. Conversely, the mole fraction of HF(3) increases the weight.

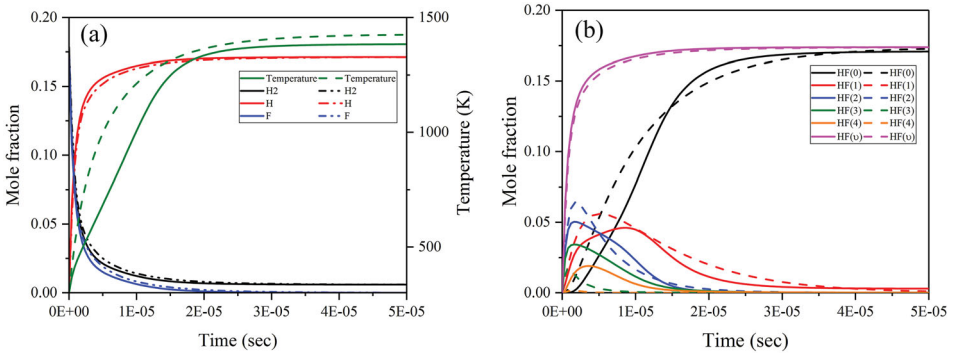

Figure 4. Time evolution of temperature profiles and distribution of species. Solid lines represent results of the detailed state-to-state model, and dashed lines those of the vibrational-resolved model [21] at initial temperature of 300 K and the initial pressure of 650 Pa. Performance of (a) temperature, H, H_2 and F, and (b) HF($\upsilon = 0$–4).

For a detailed analysis, each ro-vibrational state HF(υ, j) was reproduced based on the equation of the rotational level of equilibrium Boltzmann distribution. The probability distribution over vibrational levels is expressed as:

$$P_{\mathrm{rot}}(j) = \frac{(2j+1)\exp(-E_{\upsilon,j}/k_B T)}{\sum (2j+1)\exp(-E_{\upsilon,j}/k_B T)}, \tag{5}$$

Figure 5 illustrates that the detailed profiles of the ro-vibrational HF species are strikingly different from the assumption of equilibrium Boltzmann distribution. For the lower rotational level state of HF(2, j), the numerical results of the detailed chemical mechanism are much lower than the results of the Boltzmann model. On the contrary, the mole fractions of the higher rotational level of HF(2) are much larger than those in the Boltzmann model. Analysis of HF(3, j) shows that the maximum values of the detailed mechanism are always larger. For the Boltzmann's model, the time to reach the maximum mole fraction values is a shorter magnitude than in the detailed state-to-state model.

As described above, the detailed state-to-state model and equilibrium Boltzmann distribution model behave differently in mole fraction of HF(υ, j). It is important to note that chemical mechanism with equilibrium Boltzmann distribution does not consider the real energy transfer of each rotational level. These numerical simulations are all executed with the same initial conditions between the detailed mechanism and the skeletal mechanism, the change of temperature and number density with increasing time can affect the distribution of the ro-vibrational excited HF species. Hence, all of the above results can only show the differences between the real reaction behaviour and equilibrium Boltzmann distribution. Overall, these equilibrium Boltzmann distribution mechanisms that are used in the majority of HF chemical lasers cannot describe the real rotational energy transfer processes.

3.2. *Influence of rotational nonequilibrium*

In HF chemical lasers, models that consider rotational nonequilibrium are more successful at predicting the performance of HF chemical lasers than those with the assumption of equilibrium distribution. However, the presence of rotational nonequilibrium is still controversial on account of the lack of strong experimental evidence and detailed numerical

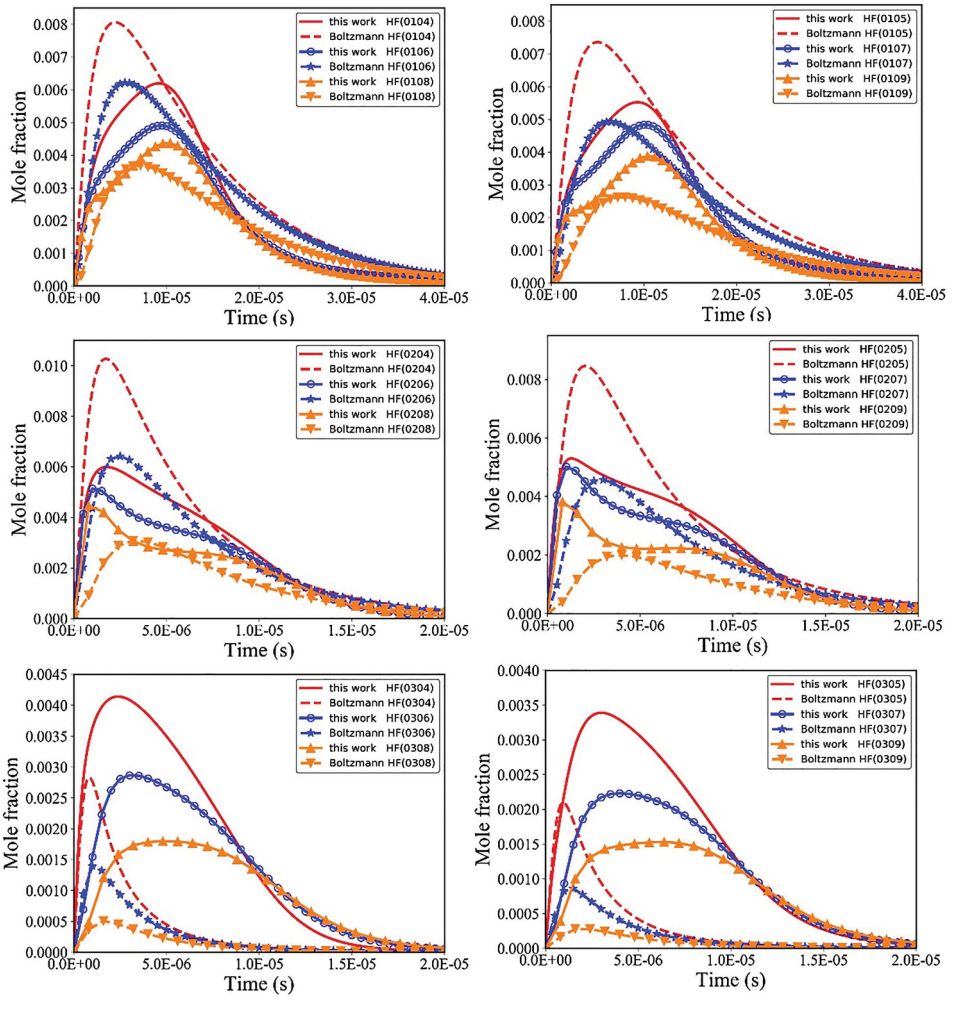

Figure 5. Mole fraction distribution of HF(2, *j*) and HF(3, *j*). Solid lines represent results of the detailed rotational state-to-state mechanism, and dashed lines those of the skeletal mechanism with the rotational Boltzmann distribution.

analysis over the past several decades [18,35]. Next, we present the effect of rotational nonequilibrium on the distribution of ro-vibrational excited HF species with detailed chemical mechanism.

From the Figures 6 and 7, it can be seen that the distributions of HF(1, *j*) and HF(2, *j*) are far from equilibrium Boltzmann distribution. However, the distributions of HF(3, *j*) and HF(4, *j*) show a good agreement with Boltzmann distribution at both temperature of 300 and 500 K. These results have good agreement with the experimental data [8,9] that non-Boltzmann distributions for excited HF(υ, *j*) molecules. In HF chemical lasers, the nonequilibrium distribution of rotational levels can significantly affect the phenomenological parameter, small signal gain, which is used to evaluate the performance of HF chemical lasers [36,37]. In this paper, we identify these rotational relaxation processes and immediate species HF(υ, *j*) distribution by using a zero-dimension reactor model.

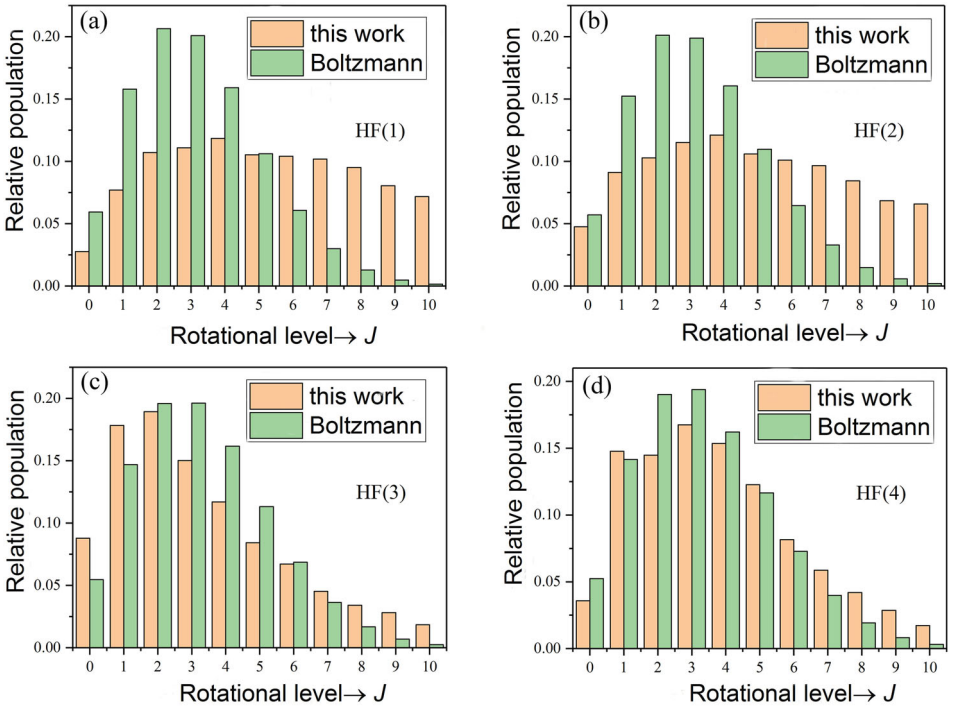

Figure 6. Comparison of rotational level distribution with Boltzmann distribution over rotational levels at $t = 1.2\text{E}-06\,\text{s}^{-1}$ and temperature of 300 K. Boltzmann distributions are recalculated based on Eq.(5) by summing of HF(υ, j) at each time step. All these results are normalised to equal unity.

When the residence time $t = 1.2 \times 10^{-6}\,\text{s}^{-1}$, the evolution of HF($\upsilon$, j) species behaves difference and rotational nonequilibrium processes clearly exist in HF chemical lasers. Due to the enormous inherent complexity of the real HF chemical lasers, further computational fluid dynamics studies with this state-to-state chemical kinetic mechanism should been conducted to investigate the affection of small signal gain and spectral distribution.

4. Conclusions

In summary, a detailed state-to-state chemical kinetic mechanism has been developed with a wide range of conditions including 61 species and 124,482 reactions. The corresponding vibrational-resolved mechanism has been updated. The rotational rate coefficients of F + H_2, HF(υ, j) + H_2 and HF(υ, j) + HF(υ', j') have been calculated with quantum chemical methods. Compared to the skeletal mechanism with the assumption of Boltzmann distribution [17], one of the main differences between the two mechanisms is the profile of ro-vibrational excited HF molecules. These numerical results show that the inherent rotational relaxation processes can significantly affect the performance of HF chemical lasers. Hence, those models that assume a Boltzmann distribution are not suitable to elucidate the detailed processes of rotational energy transfer. Simulations of homogeneous reaction processes of the detailed mechanism at various initial conditions demonstrate that the distributions of HF(3, j), and HF(4, j) show better agreement with

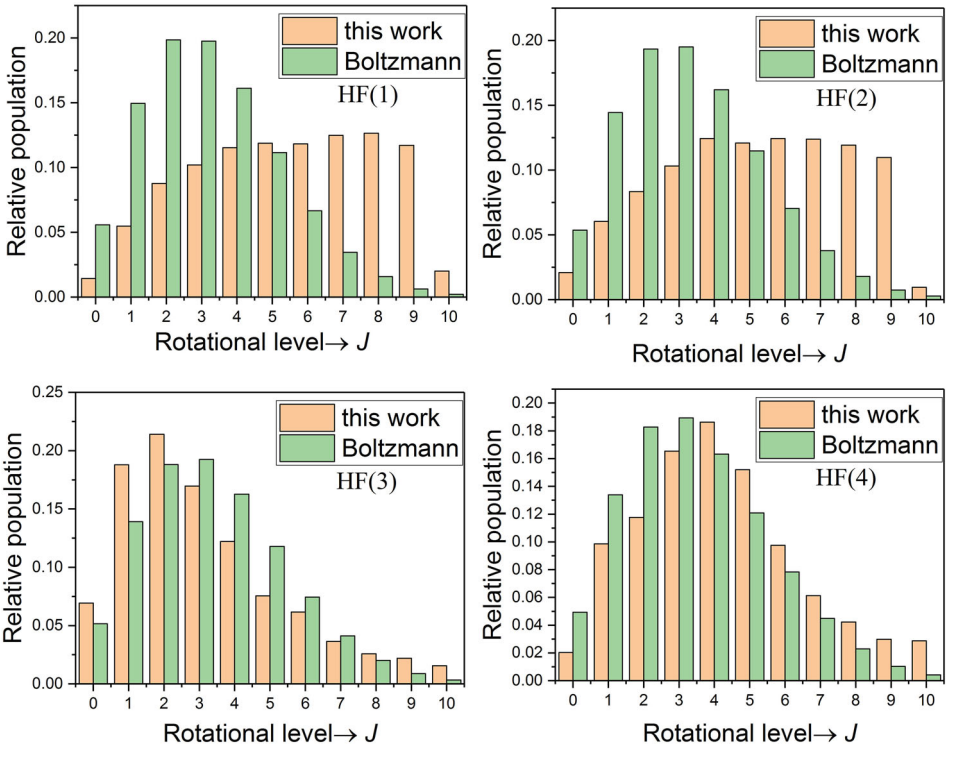

Figure 7. Comparison of rotational level distribution with Boltzmann distribution over rotational levels at $t = 1.2\text{E}-06\,\text{s}^{-1}$ and temperature of 500 K. Boltzmann distributions are recalculated based on Eq. (5) by summing of HF(υ, j) at each time step. All these results are normalised to equal unity.

Boltzmann's distribution, and that the distributions of HF(1, j), and HF(2, j) are both far from equilibrium distribution.

Acknowledgements

This work was financially supported by the Strategic Priority Research Program of the Chinese Academy of Sciences (grant number XDB17010300) and the National Natural Science Foundation of China (grant number 21573218).

Disclosure statement

No potential conflict of interest was reported by the authors.

Funding

This work was financially supported by the Strategic Priority Research Program of the Chinese Academy of Sciences (Grant Number XDB17010300) and the National Natural Science Foundation of China (Grant Number 21573218).

ORCID

Hui Li http://orcid.org/0000-0003-2670-0913

References

[1] M. Qiu, Z. Ren, L. Che, D. Dai, S.A. Harich, X. Wang, X. Yang, C. Xu, D. Xie, M. Gustafsson, R.T. Skodje, Z. Sun and D.H. Zhang, *Observation of feshbach resonances in the F + H2 → HF + H reaction*. Science 311 (2006), pp. 1440–1443.

[2] Y. Shagam, A. Klein, W. Skomorowski, R. Yun, V. Averbukh, C.P. Koch and E. Narevicius, *Molecular hydrogen interacts more strongly when rotationally excited at low temperatures leading to faster reactions*. Nat. Chem 7 (2015), pp. 921–926.

[3] A.S. Boreysho, V.M. Malkov, and A.V. Savin, *High-power supersonic chemical lasers: gas-dynamic problems of operation of mobile systems with PRS*, Proc. SPIE 7131, XVII International Symposium on Gas Flow, Chemical Lasers, and High-Power Lasers. 7131 (2008), pp. 713103.

[4] N. Cohen, J.F. Bott, M.A. Kwok, and R.L. Wilkins, *The status of rotational nonequilibrium in HF chemical lasers*, 16th Fluid and Plasmadynamics Conference (AIAA). 87 (1986).

[5] R.L. Kerber, R.C. Brown and K.A. Emery, *Rotational nonequilibrium mechanisms in pulsed H(2) + F(2) chain reaction lasers. 2: effect of VR energy exchange*. Appl Opt 19 (1980), pp. 293–300.

[6] L.H. Sentman and W. Rushmore, *Computationally efficient, rotational nonequilibrium cw chemical laser model*. AIAA. J 19 (1981), pp. 1323–1332.

[7] J.C. Polanyi and K.B. Woodall, *Energy distribution among reaction products. VI. F + H2, D2*. J Chem Phys 57 (1972), pp. 1574–1586.

[8] W.B. Chapman, B.W. Blackmon and D.J. Nesbitt, *State-to-state reactive scattering of F + H2 in supersonic jets: nascent rovibrational HF(v,J) distributions via direct IR laser absorption*. J. Chem. Phys 107 (1997), pp. 8193–8196.

[9] W.T. Rawlins, S.J. Davis, D.B. Oakes, D.X. Hammer, and G. Maislin, *Studies of HF(v,J) spatial profiles with a hyperspectral imager*, in *Gas and chemical lasers, and Applications III*, S. J. Davis and M. C. Heaven, eds. Proc. SPIE, Bellingham, Washington, Vol. 5334, 2004, pp. 137–144.

[10] W.T. Rawlins, D.B. Oakes and S.J. Davis, *Hyperspectral infrared imaging of HF(v, J) chemiluminescence and gain in chemically reacting flowfields*. J Phys Chem A 111 (2007), pp. 6860–6869.

[11] D.A. Neufeld, J. Zmuidzinas, P. Schilke and T.G. Phillips, *Discovery of interstellar hydrogen fluoride*. Astrophys. J 488 (1997), pp. L141–L144.

[12] T. Stoecklin, A. Voronin and J.C. Rayez, *Vibrational quenching of HF(v = 1,j) molecules by 3He atoms at very low energy*. Chem. Phys 294 (2003), pp. 117–127.

[13] B. Desrousseaux and F. Lique, *The rotational excitation of HF by H*. Mon. Not. R. Astron. Soc 476 (2018), pp. 4719–4724.

[14] G. Guillon and T. Stoecklin, *Rotational relaxation and excitation rates of hydrogen fluoride in collision with ortho- and para-H2*. Mon. Not. R. Astron. Soc 420 (2012), pp. 579–584.

[15] J. Huang, Y. Zhou and D. Xie, *Predicted infrared spectra in the HF stretching band of the H_2-HF complex*. J. Chem. Phys 149 (2018), pp. 094307.

[16] L.H. Sentman, *Rotational nonequilibrium in cw chemical lasers*. J. Chem. Phys 62 (1975), pp. 3523–3537.

[17] R.J. Hall, *Rotational nonequilibrium and line-selected operation in cw DF chemical-lasers*. IEEE J. Quantum. Electron 12 (1976), pp. 453–462.

[18] N. Cohen, and J.F. Bott, *A review of rate coefficients in the H_2-F_2 chemical laser system*, DTIC Document. 1976.

[19] G.C. Manke and G.D. Hager, *A review of recent experiments and calculations relevant to the kinetics of the HF laser*. J Phys Chem Ref Data 30 (2001), pp. 713–733.

[20] H. Li, S. Jia, T. Zhao and Y. Huai, *Skeletal and reduced chemical mechanism for hydrogen fluoride chemical laser*. J. Math. Chem 56 (2018), pp. 2496–2511.

[21] B. Zhao, Z. Sun and H. Guo, *Calculation of state-to-state differential and integral cross sections for atom-diatom reactions with transition-state wave packets*. J. Chem. Phys 140 (2014), pp. 234110.

[22] B. Zhao, Z. Sun and H. Guo, *A reactant-coordinate-based approach to state-to-state differential cross sections for tetratomic reactions*. J. Chem. Phys 145 (2016), pp. 184106.

[23] J. Chen, Z. Sun and D.H. Zhang, *An accurate potential energy surface for the F + H_2 → HF + H reaction by the coupled-cluster method*. J. Chem. Phys 142 (2015), pp. 024303.
[24] Z. Sun and D.H. Zhang, *Development of the potential energy surface and current stage of the quantum dynamics studies of the F + H2/HD reaction*. Int. J. Quantum. Chem 115 (2015), pp. 689–699.
[25] X. Yang and D.H. Zhang, *Dynamical resonances in the fluorine atom reaction with the hydrogen molecule*. Acc. Chem. Res 39 (2010), pp. 981–989.
[26] T. Yang, H. Long, W. Tao, C. Xiao and X. Yang, *Effect of reagent vibrational excitation on the dynamics of F + $H_2(v = 1, j = 0)$ → $HF(v', j')$ + H reaction*. J Phys Chem A 119 (2015), pp. 12284–12290.
[27] T. Wang, T. Yang, C. Xiao, Z. Sun, D. Zhang, X. Yang, M.L. Weichman and D.M. Neumark, *Dynamical resonances in chemical reactions*. Chem. Soc. Rev 47 (2018), pp. 6744–6763.
[28] D. Yang, J. Huang, J. Zuo, X. Hu and D. Xie, *A full-dimensional potential energy surface and quantum dynamics of inelastic collision process for H_2-HF*. J. Chem. Phys 148 (2018), pp. 184301.
[29] D. Yang, X. Hu and D. Xie, *Quantum dynamics of vibration-vibration energy transfer for vibrationally excited HF colliding with H2*. J. Comput. Chem 40 (2019), pp. 1084–1090.
[30] J. Huang, D. Yang, Y. Zhou and D. Xie, *A new full-dimensional ab initio intermolecular potential energy surface and vibrational states for $(HF)_2$ and $(DF)_2$*. J. Chem. Phys 150 (2019), pp. 154302.
[31] P.J. Linstrom and W.G. Mallard, *The NIST Chemistry WebBook: A chemical data resource on the internet*†. J Chem Eng Data 46 (2001), pp. 1059–1063.
[32] K.K. Irikura, *Experimental vibrational zero-point energies: diatomic molecules*. J Phys Chem Ref Data 36 (2007), pp. 389–397.
[33] R.J. Le Roy, *Improved parameterization for combined isotopomer analysis of diatomic spectra and its application to HF and DF*. J. Mol. Spectrosc 194 (1999), pp. 189–196.
[34] R.J. Kee, F.M. Rupley, and J.A. Miller, *Chemkin-II: A fortran chemical kinetics package for the analysis of gas-phase chemical kinetics*, Sandia National Labs. Livermore, CA (USA), 1989.
[35] G.C. Manke, K.B. Hewett, C.F. Wisniewski, C.R. Truman and G.D. Hager, *On the presence of rotational nonequilibrium in a supersonic hydrogen-fluoride laser*. IEEE J. Quantum. Electron 39 (2003), pp. 1625–1634.
[36] C.F. Wisniewski, K.B. Hewett, G.C. Manke II, P.G. Crowell, C.R. Truman, and G.D. Hager, *Small signal gain measurements in a small scale HF overtone laser*, Appl Phys A. 77 (2003), pp. 337–342.
[37] C.F. Wisniewski, K.B. Hewett, G.C. Manke, C.R. Truman and G.D. Hager, *Hydrogen fluoride overtone laser: 2D CFD modeling of the small signal gain*. Proc. SPIE Int. Soc. Opt. Eng 5448 (2004), pp. 1127–1138.